Monthly Notices
of the
ROYAL ASTRONOMICAL SOCIETY

MNRAS **428,** 3048–3057 (2013) doi:10.1093/mnras/sts252

Extragalactic point source detection in *Wilkinson Microwave Anisotropy Probe* 7-year data at 61 and 94 GHz

L. F. Lanz,[1,2]★ D. Herranz,[1,3] M. López-Caniego,[1] J. González-Nuevo,[4] G. de Zotti,[4,5] M. Massardi[5,6] and J. L. Sanz[1]

[1]*Instituto de Física de Cantabria, CSIC-UC, Av. de Los Castros s/n, Santander E-39005, Spain*
[2]*Departamento de Física Moderna, Universidad de Cantabria, Av. de Los Castros s/n, Santander E-39005, Spain*
[3]*Astrophysics Group, Cavendish Laboratory, JJ Thomson Avenue, Cambridge CB3 0HE*
[4]*SISSA, via Bonomea 265, I-34136 Trieste, Italy*
[5]*INAF – Osservatorio Astronomico di Padova, Vicolo dell'Osservatorio 5, I-35122 Padova, Italy*
[6]*INAF – Istituto di Radioastronomia, Via P. Gobetti 101, I-40129 Bologna, Italy*

Accepted 2012 October 19. Received 2012 September 27; in original form 2011 October 31

ABSTRACT

The detection of point sources in cosmic microwave background maps is usually based on a single-frequency approach, whereby maps at each frequency are filtered separately and the spectral information on the sources is derived combining the results at the different frequencies. In contrast, in the case of multifrequency detection methods, source detection and spectral information are tightly interconnected in order to increase the source detection efficiency.

In this work we apply the *matched multifilter* method to the detection of point sources in the *Wilkinson Microwave Anisotropy Probe* (*WMAP*) 7-year data at 61 and 94 GHz. This linear filtering technique takes into account the spatial and the cross-power spectrum information at the same time using the spectral behaviour of the sources without making any a priori assumption about it. We follow a two-step approach. First, we do a blind detection of the sources over the whole sky. Secondly, we do a refined local analysis at their positions to improve the signal-to-noise ratio of the detections. At 94 GHz we detect 129 5σ objects at $|b| > 5^\circ$ (excluding the Large Magellanic Cloud region); 119 of them are reliable extragalactic sources and 104 of these 119 lie outside the *WMAP* Point Source Catalogue mask. Nine of the total 129 detections are known Galactic sources or lie in regions of intense Galactic emission and one additional (weak) high Galactic latitude source has no counterpart in low-frequency radio catalogues. Our results constitute a substantial improvement over the New Extragalactic WMAP Point Source (NEWPS) 3-year catalogue.

Key words: methods: data analysis – techniques: image processing – surveys – radio continuum: galaxies – cosmic background radiation.

1 INTRODUCTION

The study of the cosmic microwave background (CMB) provides a very useful tool in understanding the Universe and its evolution. A proper analysis of this primordial radiation allows us to discriminate between different evolutionary models of the Universe. Different experiments have taken data with different observing conditions (i.e. resolutions, frequencies, fields of view, etc.) in order to improve our comprehension of this radiation and, therefore, of the Universe. The excellent sensitivities of modern instruments, close to fundamental limits, imply that our ability to accurately measure the CMB temperature anisotropies is limited by the contamination of CMB maps by astrophysical emissions (foregrounds). For this reason, many techniques have been developed in order to separate the different components that one can find in the maps. While on moderate to large angular scales the main contaminants are diffuse Galactic emissions, extragalactic point sources dominate on small angular scales both in temperature (Toffolatti et al. 1998; De Zotti et al. 1999, 2005; Hobson et al. 1999) and in polarization (Tucci et al. 2004, 2005; López-Caniego et al. 2009; Argüeso, Sanz & Herranz 2011a).

Astrophysical foregrounds can be both a disturbance for CMB studies and interesting per se. The *Wilkinson Microwave Anisotropy Probe* (*WMAP*) surveys have made it possible to investigate for the first time the statistical properties of bright radio sources above

★E-mail: lanz@ifca.unican.es

© 2012 The Authors
Published by Oxford University Press on behalf of the Royal Astronomical Society

Downloaded from http://mnras.oxfordjournals.org/ at CSIC on January 9, 2015

$\sim$10 GHz over the whole sky (Bennett et al. 2003; Hinshaw et al. 2007; López-Caniego et al. 2007; Chen & Wright 2008; González-Nuevo et al. 2008; Massardi et al. 2009; Wright et al. 2009; Gold et al. 2011). The first *Planck* results (Planck Collaboration 2011a) have already offered the possibility of extending the study to higher frequencies and fainter flux densities (Planck Collaboration 2011b).

There is a rich literature on methods to extract compact sources from CMB maps (see Herranz & Vielva 2010, for a recent review). Successful techniques exploit a variety of tools: wavelets (Vielva et al. 2001, 2003; González-Nuevo et al. 2006; Sanz et al. 2006; López-Caniego et al. 2007), matched filters (Vikhlinin et al. 1995; Tegmark & de Oliveira-Costa 1998; Barreiro et al. 2003; López-Caniego et al. 2006) and other linear filtering tools (Sanz, Herranz & Martínez-Gónzalez 2001; Chiang et al. 2002; Herranz et al. 2002a; López-Caniego et al. 2004, 2005a,b). Usually, these methods filter maps at each frequency separately. In addition, Bayesian techniques that include prior information about the distribution of the sources have been proposed in the literature (Hobson & McLachlan 2003; Carvalho, Rocha & Hobson 2009; Argüeso et al. 2011b).

Although single-frequency filtering techniques have been remarkably successful, a multifrequency approach allows us to take advantage of additional information such as the cross-power spectrum of the noise. This makes it possible to improve the significance of sources seen at different frequencies but with relatively low signal-to-noise ratio (S/N) in each frequency channel without any a priori assumption on their spectral properties. However, multifrequency detection of point sources in CMB maps is still a poorly explored field. Herranz & Sanz (2008) introduced the matrix filters (MTXF) technique as the first fully multifrequency, non-parametric, linear filtering technique that is able to find point sources and do unbiased estimations of their flux densities. The MTXF technique exploits the distinctive spatial behaviour of these sources without assuming any specific spectral behaviour. Herranz et al. (2009) applied the MTXF technique to realistic simulations of the *Planck* radio channels, showing that it is possible to practically double the number of detections for some of the channels with respect to the single-frequency matched filter approach for a fixed reliability level.

The MTXF approach exploits the multifrequency information only on the diffuse components (like CMB, Galactic emissions and noise). A more complete approach should also take into account the correlations among the different frequency maps due to point sources themselves. A step in this direction was done by Herranz et al. (2002b) who presented the matched multifilter (MMF) method, a generalization of the standard matched filter for multifrequency data where the frequency dependence of the signal is known. This is the case for the thermal Sunyaev–Zel'dovich (SZ) effect (Sunyaev & Zeldovich 1970, 1972), for which the method was originally developed and which has been used to build the *Planck* Early SZ catalogue. Unfortunately, this is not the case for extragalactic radio sources. However, Lanz et al. (2010) took advantage of an analogy between the SZ and the point source case. In the SZ case, the spectral behaviour of the sources is known, but the size of the clusters is not. To deal with this, the size of the source is described, in the design of an MMF, by means of a free parameter, whose value is determined maximizing the S/N for each detected source (Herranz et al. 2002b). In the case of point sources, the angular profiles are known [they are given by the point spread functions (PSFs) of the instrument], and we only need to optimize a set of parameters describing the spectral shape.

In Lanz et al. (2010), the MMF was applied to realistic simulations of the *Planck* mission. The promising results obtained in that work prompted us to apply the method to real data, namely to the *WMAP* 7-year data. More precisely, we have considered the *V* and *W* maps (61 and 94 GHz, respectively), because at these frequencies the knowledge of the statistical properties of radio galaxies was poor. The structure of the article is as follows. In Section 2 we briefly describe the method, and in Section 3 the data used. In Section 4 we present and discuss our results, comparing our flux density estimates with measurements with other instruments. Our main conclusions are summarized in Section 5.

2 METHOD

The MMF is the optimal linear detection method when the spatial profile and the frequency dependence of the sources are known. By 'optimal' we mean, as it is common in statistics, that the estimation of the flux density of the sources is unbiased and has minimum variance (maximum efficiency). In Fourier space the MMF takes the form

$$\boldsymbol{\Psi}(q) = \alpha\, \mathbf{P}^{-1}\boldsymbol{F}, \quad \alpha^{-1} = \int \mathrm{d}\boldsymbol{q}\; \boldsymbol{F}^{\mathrm{T}}\mathbf{P}^{-1}\boldsymbol{F}, \tag{1}$$

where q is the Fourier mode, $\boldsymbol{\Psi}(q)$ is the column vector of the filters $\boldsymbol{\Psi}(q) = [\psi_\nu(q)]$, $\boldsymbol{F}$ is the column vector $\boldsymbol{F} = [f_\nu \tau_\nu]$, f_ν is the frequency dependence, $\tau_\nu(q)$ is the source profile at each frequency ν and $\mathbf{P}^{-1}$ is the inverse matrix of the cross-power spectrum $\mathbf{P}$. The MMF takes as arguments N images (in this work $N = 2$) and returns a single filtered image where the sources are optimally enhanced with respect to the noise. The variance of the output-filtered image is given by

$$\sigma^2 = \int \mathrm{d}\boldsymbol{q}\, \boldsymbol{\Psi}^{\mathrm{T}}\mathbf{P}\boldsymbol{\Psi} = \alpha. \tag{2}$$

If a source has a S/N ≥ 5 after the filtering, we say that we have a detection at that position.

Since we are dealing with point sources, the profiles τ_ν are directly given by the PSFs of the instrument. The cross-power spectrum $\mathbf{P}$ is not known a priori but can be inferred from the data under the assumption that the point sources are sparse. The unknown frequency dependence, $\boldsymbol{f} = [f_\nu]$, of a given source can be parametrized as

$$\frac{S_\nu}{S_0} = \left(\frac{\nu}{\nu_0}\right)^\gamma, \tag{3}$$

where S_ν and S_0 are the flux densities at a frequency ν and at the frequency of reference ν_0. The spectral index γ is a free parameter. As pointed out by Lanz et al. (2010), each image is filtered several times for different MMFs. These MMFs are identical except for the spectral index γ. The test values of the spectral index used in this work are $-3.5 \leq \gamma \leq 3.5$, with a step of 0.05. As it was shown in the cited work, the S/N of the detected source is maximal for the correct choice of this parameter, and by construction (we want an *efficient* estimator of the flux density of the source), the uncertainty assigned to the source is the square root of the variance expressed in equation (2) for the correct value of γ. While the parametrization of equation (3) is perfectly adequate in our case, any other parametrization, even a non-functional description of the vector $\boldsymbol{f}$ by means of its components, could be used in other cases, for example, when more than two frequencies are considered simultaneously.

3 APPLICATION TO *WMAP* DATA

As mentioned above, the *WMAP V* and *W* bands are particularly interesting because only a small fraction of *WMAP* sources were

Downloaded from http://mnras.oxfordjournals.org/ at CSIC on January 9, 2015

detected with S/N $\geq 5\sigma$ in these bands. We have used an adapted version of the code described in López-Caniego et al. (2007, 2009) and Massardi et al. (2009), modified in order to handle two frequencies simultaneously and to accommodate our MMF filtering. The code reads in an input parameter file containing the specific characteristics of the maps to be analysed as well as the patch size, the pixel size and overlap among the patches to effectively cover the 100 per cent of the sky. Then, it reads in the two input maps in Flexible Image Transport System (FITS) format and extracts the patches to be analysed using the tangential plane approximation implemented in the CPACK library.[1] Each pair of *V* and *W* patches is analysed simultaneously using the MMF, and a first set of detections is produced. Next, the code iteratively explores different values of the spectral index for each source, allowing for the appearance of new possible detections. At the end, the code gathers all the candidates and generates a list of detections above a given S/N, converting the positions of the detected objects in the plane to the sphere. We have used flat patches of $14.^{\circ}6 \times 14.^{\circ}6$, each containing 128×128 pixels. The pixel area is $6.871 \times 6.871\,\mathrm{arcmin}^2$, corresponding to the HEALPIX resolution parameter $N_{\mathrm{side}} = 512$ (see Górski et al. 2005, for more details). In total we have 371 patches, with significant overlaps among them in order to avoid as much as possible border effects. As described in Massardi et al. (2009), we perform a two-step process, first doing a blind search across the sky and then refining the analysis obtaining new patches centred at the positions of the sources identified in the blind step. In this way we further reduce any projection and border effect that we could have.

When dealing with the *V* and especially the *W WMAP* bands, it is necessary to carefully characterize the properties of the beams, both to build the optimal filters (equation 1) and to obtain a good photometry of the sources. *WMAP* beams, particularly at 94 GHz, are highly non-Gaussian. We also need to take into account that for the *W* band the pixel size (6.871 arcmin) is dangerously close to the minimum sampling of the full width at half-maximum required to avoid aliasing and that real sources are not necessarily located at the geometrical centre of the pixels. We have dealt with these systematic effects in the following way.

We used the beam transfer functions (circularly symmetric) provided by *WMAP*[2] to create high-resolution templates of the beams (equivalent to the HEALPIX $N_{\mathrm{side}} = 4096$) projected into the tangent plane. The maps that we have used to perform our analysis have a pixel size corresponding to $N_{\mathrm{side}} = 512$. However, as we said before, we must consider that sources are not necessarily located at the geometrical centre of these $N_{\mathrm{side}} = 512$ pixels. Therefore, taking the beam transfer functions, we divided each $N_{\mathrm{side}} = 512$ pixels into 8×8 subpixels ($N_{\mathrm{side}} = 4096$). Then, we put the maximum of the high-resolution beam template in each 8×8 possible positions for each $N_{\mathrm{side}} = 4096$ subpixels. In order to obtain a well-estimated average of the beams, we repeated the process described in this paragraph 5000 times and averaged over the beam templates we obtained. These effective beam templates were then degraded to the same resolution of our maps ($N_{\mathrm{side}} = 512$). In this way we take into account, on average, the effects of pixelization and the possible offsets of the sources with respect to the geometrical centre of the pixel.

A careful correction for the non-circularity of the beams would require a detailed knowledge of the combination of beam orientations for all scans through every position in the sky. Since this information is not available to us, and hence it is impossible to solve the problem of non-circularity, we only applied to the flux densities an average correction factor that takes into account the effective beam areas for each channel. The correction factors were obtained using the self-calibration method based on SEXTRACTOR (Bertin & Arnouts 1996) AUTO photometry, described in González-Nuevo et al. (2008). In that work, the NEWPS 3-year sources detected above the 5σ level by SEXTRACTOR and with flux densities $S \geq 1$ Jy were used for self-calibration. Only three *W*-band sources satisfied these requirements and therefore the correction factor for this band could not be reliably estimated. To overcome this problem we have applied SEXTRACTOR to the *W* map at the positions of 296 sources observed by the Australia Telescope Compact Array (ATCA) and the Very Large Array (VLA). 15 of them were detected at $\geq 3\sigma$ by SEXTRACTOR. Since all the ATCA/VLA sources have been detected at a very high significance level, we were confident that there were no spurious detections in this sample. These sources were used to recalculate the effective beam area at 94 GHz. We obtained $(2.50 \pm 0.09) \times 10^{-5}$ sr to be compared with the nominal value of 2.07×10^{-5} sr for the symmetrized beam. Note that all the ingredients described in this section must be introduced in the code before the filtering process.

4 RESULTS AND DISCUSSION

The source detection was performed applying the MMF filter to the 7-year *WMAP V* and *W* maps, at 61 and 94 GHz, respectively. We have used only one (*V*1) of the two differencing assemblies for the *V* band, because *V*1 and *V*2 are very similar. As for the *W* band, we used two (*W*2 and *W*3) out of the four differencing assemblies because their symmetrized beam profiles are geometrically very similar (same as for *W*1 and *W*4), and this makes the photometry easier. The *W*2 and *W*3 maps were combined pixel by pixel, weighting with the inverse of the variances of the pixels. To minimize the spurious detections due to the complex structures of the Galactic emissions near the equatorial plane and of the Large Magellanic Cloud (LMC) region, we have removed from the final catalogue objects with $|b| \leq 5^{\circ}$ and within a radius of 5° around the LMC [$(80.^{\circ}894, -69.^{\circ}756)$ in equatorial coordinates]. No sources are detected within the Small Magellanic Cloud.

4.1 Point source detection

The two-step filtering approach described in Section 3 yields 129 5σ detections in the 61- and 94-GHz *WMAP* 7-year maps, outside the Galactic plane and LMC regions specified above. For each of them, the MMF gives the flux density at the reference frequency (94 GHz, ν_0 in equation 3) and the spectral index, the only free parameter of the method. The uncertainty on the spectral index can be estimated from intensive simulations made in Lanz et al. (2010). Table 1 lists the nine sources that are either well-known Galactic sources (like the Crab nebula, the H II regions NGC 281 and NGC 1499 or the star formation regions NGC 1333 and NGC 6729) or located within Galactic molecular cloud complexes, like the Orion or the Ophiucus regions, or within regions of intense Galactic emissions, plus one unidentified source. Table 1 gives the flux densities within the *WMAP* 94-GHz beam. In most cases, these are lower limits to the total flux densities because the sources are resolved. Given the different beam sizes at the two frequencies, the spectral indices cannot be reliably estimated in the case of resolved sources.

[1] http://astro.ic.ac.uk/~mortlock/cpack/
[2] lambda.gsfc.nasa.gov/product/map/dr4/beam_xfer_get.cfm

Downloaded from http://mnras.oxfordjournals.org/ at CSIC on January 9, 2015

Table 1. Equatorial coordinates and identifications of the Galactic or unidentified detections. Sources without data are detections that, due to the multifrequency method, do not have a clear estimation of their flux density of the spectral index inside the studied range of γ.

RA (°)	Dec. (°)	$S_{94\,\mathrm{GHz}}$ (Jy beam^{-1})	*rms* (Jy)	Spectral index	ID in other catalogues
13.237	56.576	2.86	0.22	−1.25	NGC 281
44.622	−18.834	0.54	0.10	−2.40	–
52.264	31.338	4.81	0.57	4.50	NGC 1333
60.731	36.189	0.49	0.09	−3.35	NGC 1499
83.654	22.045	155	2	−1.15	Crab nebula
83.807	−5.419	216	3	−0.35	Orion region
84.018	−6.338	–	–	–	Orion region
85.396	−1.917	30	2	−0.2	Orion region
246.756	−24.633	–	–	–	Ophiucus region
285.398	−36.983	3.31	0.55	3.70	NGC 6729

Excluding the 10 sources listed in Table 1, the MMF has detected 119 objects, listed in Table 2. All these objects have a counterpart in lower frequency radio catalogues, which cover the whole sky to much fainter flux density limits[3] (see Fig. 1). The apparently ultrasteep ($\gamma_{61}^{94} = -2.25$) spectrum of Cygnus A is partly due to resolution effects (the 94-GHz beam encompasses a lower fraction of the total flux density than the 61-GHz beam).

In Tables 1 and 2, sources without an estimation of the flux density or the spectral index are objects that are only 'detected' at one frequency. Therefore, because the method we use to filter the maps is multifrequency, the spectral indices of these sources fall outside the range studied in this work. These sources are not taken into account in the subsequent analysis.

The spectral index distribution of the sources in Table 2, shown in Fig. 2, has a median value of −0.65 with a dispersion of 0.71. For comparison, Wright et al. (2009), mostly based on lower frequency *WMAP* data, found a mean spectral index $\langle\gamma\rangle = -0.09$, with a dispersion $\sigma = 0.28$. Our results are therefore consistent with the steepening of source spectra above ∼70 GHz found for different data sets (González-Nuevo et al. 2008; Sadler et al. 2008; Massardi et al. 2010; Marriage et al. 2011; Planck Collaboration 2011b).

The Euclidean normalized source counts at 61 and 94 GHz are given in Table 3 and shown in Fig. 3, where they are compared with the counts in the nearest *Planck* channels (Planck Collaboration 2011b) and with the predictions of the De Zotti et al. (2005) and Tucci et al. (2011) models.

In this figure, the flux densities obtained with the MMF were corrected with a Bayesian approach (Herranz et al. 2006) in order to remove as much as possible the Eddington bias (Eddington 1913). This approach takes into account the distribution in flux density of the objects as a power law with unknown slope, and an additive Gaussian noise. It is important to point out that this correction is statistical, and therefore it has been taken into account only in the estimation of the source counts.

The comparison in Fig. 3 shows that our completeness limit is ≃2 Jy. Above this limit, the agreement with the *Planck* counts and with the Tucci et al. (2011) model is generally good. This confirms that the Tucci et al. (2011) model deals appropriately with the high-frequency behaviour of source spectra.

Although several data sets had suggested (González-Nuevo et al. 2008; Sadler et al. 2008) and then detected (Planck Collaboration 2011b,c) a break in the bright extragalactic radio sources (at high-flux level) at ∼70 GHz, this break is only well explained with the current data if we consider the Tucci et al. (2011) model.

4.2 Comparison with the *WMAP* catalogues

The *WMAP* Five-Band Point Source Catalogue (Gold et al. 2011) lists all the sources that were detected at $\geq 5\sigma$ in at least one frequency channel, outside a mask excluding sources in the Galactic plane and Magellanic Cloud regions. Flux densities in the other channels are reported if the signal is detected at a significance $>2\sigma$. In this catalogue, 94-GHz flux densities are reported for 236 sources; 59 of them are detected at a $\geq 5\sigma$ level at 94 GHz. By contrast, our method guarantees that all the 119 (presumably) extragalactic sources, 104 of which are outside the *WMAP* Point Source Catalogue mask, are detected at $\geq 5\sigma$ at 94 GHz.

4.3 Comparison with NEWPS catalogues

López-Caniego et al. (2007) looked for sources in the *WMAP* 3-year maps at the positions of known 5-GHz sources (non-blind search) and reported 22 detections at 94 GHz (listed in the NEWPS 3-year catalogue). Massardi et al. (2009) combined a non-blind (based on the ATCA 20-GHz survey catalogue) and a blind search on *WMAP* 5-year maps, excluding the *W* (94 GHz) channel (NEWPS 5-year catalogue). At 61 GHz they detected 169 sources, 61 of which are not present in our catalogue (if we also take into account Table 1); 45 of them, however, are detected at $\geq 3\sigma$ with the MMF in the blind step of our detection process. Seven of the other 18 sources are at $|b| < 15^\circ$ and may be contaminated by Galactic emission, and three lie in the LMC region, excluded from our search. The remaining eight sources have not been detected by the MMF. On the other hand, our catalogue of extragalactic objects contains 16 sources not present in the NEWPS 5-year catalogue. We must remark that our catalogue is completely based on a blind search, whereas the NEWPS catalogue was guided by a previous selection of sources detected at low frequency.

4.4 Comparison with ATCA and NRAO flux densities

Our sample of 94-GHz detections includes 85 sources with ground-based ≃3 mm observations either with ATCA[4] or with the NRAO 12-m telescope (Holdaway, Owen & Rupen 1994).[5] The ATCA

[3] Except for a few of the sources in Table 1, none of the objects detected by the MMF has an *IRAS* counterpart.

[4] http://www.narrabri.atnf.csiro.au/calibrators/index.html

[5] http://www.alma.nrao.edu/memos/html-memos/alma123/memo123.pdf

Downloaded from http://mnras.oxfordjournals.org/ at CSIC on January 9, 2015

flux densities for these sources have been collected in the frequency range between 85 and 105 GHz with the 'old' ATCA digital correlator with up to 2 × 256 MHz bandwidth.

The MMF flux density estimates are compared with ATCA and NRAO measurements in Fig. 4. There is evidence that the MMF somewhat overestimates the flux densities below $\simeq$2 Jy, most likely due to the Eddington bias. Above 2 Jy the mean absolute fractional error $\langle |S_{\rm MMF} - S_{\rm ground}|/S_{\rm ground}\rangle \simeq 38$ per cent, somewhat higher than expected from the combination of nominal measurement errors and variability, suggesting that the true errors associated with the MMF flux density estimates are somewhat larger than the nominal values. In this respect, it must be noted that the *WMAP* 7-year maps are averages over 7 years of observations, while the ATCA and NRAO measurements refer to a single epoch.

Table 2. Sources detected by the MMF on *WMAP* 7-year maps with counterparts in lower frequency catalogues. Presumably Galactic sources are listed in Table 1. The equatorial coordinates (first two columns) are in degrees. The flags in the last column indicate if the source is listed in any of the *WMAP* 7-year catalogues at any frequency (W) (Gold et al. 2011), in NEWPS 5-year catalogue at 61 GHz (N) (Massardi et al. 2009) or in the *Planck* catalogue at 70 or 100 GHz (P) (Planck Collaboration 2011a). Sources without data are detections that, due to the multifrequency method, do not have a clear estimation of their flux density of the spectral index inside the studied range of γ. These sources with no flux density information are not taken into account in the subsequent analysis.

RA (°)	Dec. (°)	$S_{94\,\rm GHz}$ (Jy beam^{-1})	*rms* (Jy)	Spectral index	ID in other catalogues	Flags
1.483	−6.350	1.30	0.23	−0.80	PMN J0006−0623	WNP
5.033	73.493	1.41	0.26	−0.45	GB6 J0019+7327	P
6.514	−35.154	0.72	0.14	−1.65	PMN J0026−3512	WN
9.603	−24.892	1.65	0.33	0.30	PMN J0038−2459	WNP
16.715	−40.600	1.74	0.21	−0.55	PMN J0106−4034	WNP
23.160	−16.928	0.91	0.17	−1.20	PKS 0130−17	WNP
24.279	47.846	1.91	0.19	−1.20	GB6 J0136+4751	WNP
24.383	−24.518	1.56	0.30	0.20	PMN J0137−2430	WNP
32.749	−51.070	1.93	0.17	−1.00	PMN J0210−5101	WNP
34.293	73.803	0.73	0.13	−1.70	GB6 J0217+7349	NP
39.510	28.836	2.20	0.33	−0.20	GB6 J0237+2848	WNP
39.723	16.654	–	–	–	GB6 J0238+1637	WP
43.374	−54.666	1.56	0.20	−0.55	PMN J0253−5441	WNP
46.088	−62.233	1.31	0.25	0.05	PMN J0303−6211	WNP
49.957	41.450	2.67	0.16	−1.90	GB6 J0319+4130	WNP
50.377	−37.092	0.81	0.14	−1.55	Fornax A	NP
53.549	−40.203	1.47	0.25	−0.20	PMN J0334−4008	WNP
54.252	32.327	2.57	0.42	0.70	GB6 J0336+3218	P
54.862	−1.734	2.33	0.33	0.05	PMN J0339−0146	WNP
57.187	−27.832	1.36	0.26	0.00	PMN J0348−2749	WNP
61.062	−36.120	2.14	0.21	−0.65	PMN J0403−3605	WNP
64.548	38.025	1.96	0.16	−2.15	3C 111	NP
65.845	−1.374	3.39	0.25	−1.15	PMN J0423−0120	WNP
67.166	−37.869	1.66	0.29	0.05	PMN J0428−3756	WNP
68.301	5.418	3.51	0.41	0.50	GB6 J0433+0521	WNP
72.260	−81.053	1.61	0.28	0.25	PMN J0450−8100	WNP
73.914	−46.248	3.05	0.26	−0.50	PMN J0455−4616	WNP
74.270	−23.427	1.66	0.20	−0.75	PMN J0457−2324	WNP
78.849	−45.994	1.02	0.19	−1.40	PMN J0515−4556	WP
79.975	−45.795	2.30	0.21	−1.20	PMN J0519−4546	WNP
80.849	−36.456	2.57	0.19	−1.05	PMN J0522−3628	WNP
84.678	−44.028	3.15	0.21	−1.15	PMN J0538−4405	WNP
91.968	−6.396	7.99	0.49	0.40	PKS 0605−06	NP
92.460	−15.756	1.79	0.24	−0.50	PMN J0609−1542	WNP
97.363	−19.946	1.66	0.32	0.55	PMN J0629−1959	WNP
98.985	−75.242	2.03	0.19	−0.80	PMN J0635−7516	WNP
101.703	44.896	1.80	0.33	0.05	GB6 J0646+4451	WNP
102.564	−16.699	1.75	0.26	−0.35	PKS 0648−16	NP
110.556	71.313	2.15	0.26	−0.05	GB6 J0721+7120	WNP
111.493	−0.972	2.23	0.38	0.65	PMN J0725−0054	WP
114.856	1.724	0.96	0.18	−1.35	GB6 J0739+0136	WNP
117.689	12.478	2.04	0.23	−0.90	GB6 J0750+1231	WNP
126.524	3.272	1.27	0.22	−0.90	GB6 J0825+0309	WNP
129.076	−20.280	1.07	0.19	−1.10	PMN J0836−2017	WNP
130.356	70.885	0.91	0.15	−1.30	GB6 J0841+7053	WNP
133.730	20.128	2.48	0.29	−0.70	GB6 J0854+2006	WNP
140.233	44.738	0.89	0.14	−2.00	GB6 J0920+4441	WP

Downloaded from http://mnras.oxfordjournals.org/ at CSIC on January 9, 2015

Table 2 – *continued*

RA (°)	Dec. (°)	$S_{94\,\mathrm{GHz}}$ (Jy beam^{-1})	*rms* (Jy)	Spectral index	ID in other catalogues	Flags
140.441	−26.324	1.07	0.21	−0.85	PMN J0921−2618	WP
141.810	38.974	2.63	0.21	−1.15	GB6 J0927+3902	WNP
159.372	−29.584	1.29	0.22	−0.75	PMN J1037−2934	WNP
159.659	5.136	0.80	0.16	−1.70	GB6 J1038+0512	W
164.323	−80.083	1.65	0.19	−0.85	PMN J1058-8003	WNP
164.615	1.562	2.86	0.22	−1.10	GB6 J1058+0133	WNP
171.870	−18.836	0.97	0.19	−1.20	PMN J1127−1857	WP
176.717	−38.190	0.92	0.15	−1.75	PMN J1147−3812	WNP
178.285	49.483	1.47	0.19	−0.70	GB6 J1153+4931	WNP
179.831	29.192	1.21	0.22	−0.60	GB6 J1159+2914	WNP
187.270	2.104	10.71	0.33	−1.20	GB6 J1229+0202	WNP
187.699	12.338	5.99	0.26	−1.05	GB6 J1230+1223	WNP
191.732	−25.848	–	–	–	PKS 1244−255	WNP
193.992	−5.821	8.59	0.32	−1.15	PMN J1256−0547	WNP
194.823	51.645	1.37	0.25	0.05	GB6 J1259+5141	W
197.630	32.472	0.82	0.13	−1.75	GB6 J1310+3220	WNP
201.390	−42.960	16.92	0.46	−1.20	Centaurus A	NP
204.426	−13.021	4.96	0.29	−0.60	PMN J1337−1257	WNP
209.267	19.351	1.39	0.21	−0.75	GB6 J1357+1919	WNP
214.876	54.421	1.05	0.20	−0.50	GB6 J1419+5423	WNP
216.967	−42.070	1.75	0.23	−0.75	PMN J1427−4206	WNP
229.382	−24.370	2.31	0.28	−0.40	PMN J1517−2422	WNP
237.415	2.563	1.54	0.27	−0.55	GB6 J1549+0237	WNP
237.763	5.461	1.77	0.26	−0.50	GB6 J1550+0527	WNP
243.420	34.145	2.58	0.25	−0.30	GB6 J1613+3412	WNP
244.386	−77.279	1.07	0.16	−1.20	PMN J1617−7717	WNP
246.561	−29.832	1.91	0.30	−0.40	PKS 1622−29	NP
248.816	38.155	3.25	0.25	−0.50	GB6 J1635+3808	WNP
249.747	57.392	1.98	0.29	0.55	GB6 J1638+5720	WNP
250.551	68.974	0.80	0.08	−2.45	GB6 J1642+6856	WNP
250.742	39.825	3.89	0.23	−0.75	GB6 J1642+3948	WNP
260.115	−1.025	2.18	0.27	−0.40	PKS 1717−00	NP
260.873	−65.025	1.32	0.25	−0.25	PMN J1723−6500	WP
263.303	−13.051	3.05	0.29	−0.30	PKS 1730−13	NP
263.593	38.888	1.08	0.20	−0.70	GB6 J1734+3857	WNP
265.933	−3.813	2.55	0.22	−0.90	PKS 1741−03	NP
267.966	9.655	4.05	0.26	−0.45	GB6 J1751+0938	WNP
268.340	28.738	1.65	0.21	−0.50	GB6 J1753+2847	WNP
270.301	78.459	1.05	0.17	−1.00	NVSS J180045+782804	WP
270.400	44.088	1.40	0.22	−0.45	GB6 J1801+4404	WNP
271.711	69.794	1.34	0.20	−0.25	GB6 J1806+6949	WNP
277.443	48.800	1.07	0.13	−1.60	GB6 J1829+4844	WNP
280.720	68.162	0.82	0.14	−0.90	GB6 J1842+6809	WP
282.241	67.063	0.84	0.13	−1.15	GB6 J1849+6705	WNP
287.737	−20.060	2.12	0.34	0.10	PMN J1911−2006	WNP
290.987	−21.081	1.50	0.25	−0.65	PMN J1923−2104	WNP
291.214	−29.282	7.01	0.28	−1.00	PMN J1924−2914	WNP
292.018	73.976	1.56	0.15	−1.20	GB6 J1927+7357	WNP
299.461	−38.755	2.04	0.26	−0.55	PMN J1957−3845	WNP
299.942	40.752	6.02	0.36	−2.25	Cygnus A	NP
300.337	−17.769	0.84	0.16	−1.60	PMN J2000−1748	WNP
302.849	−15.774	1.45	0.29	−0.25	PMN J2011−1546	WNP
314.018	−47.226	1.87	0.25	−0.45	PMN J2056−4714	WNP
323.562	−1.791	1.25	0.22	−1.00	PMN J2134−0153	WNP
324.128	0.682	1.67	0.28	−0.30	GB6 J2136+0041	WNP
327.069	6.999	3.98	0.23	−1.15	GB6 J2148+0657	WNP
327.945	−30.455	1.44	0.24	−0.55	PMN J2151−3028	WNP
328.366	47.275	1.93	0.26	−0.25	GB6 J2153+4716	NP
329.184	−69.703	1.81	0.22	−0.50	PMN J2157−6941	WNP

Downloaded from http://mnras.oxfordjournals.org/ at CSIC on January 9, 2015

Table 2 – *continued*

RA (°)	Dec. (°)	$S_{94\,\mathrm{GHz}}$ (Jy beam^{-1})	*rms* (Jy)	Spectral index	ID in other catalogues	Flags
330.649	42.251	2.68	0.25	−0.30	GB6 J2202+4216	WNP
330.745	31.724	1.66	0.28	−0.05	GB6 J2203+3145	WNP
330.851	17.436	1.24	0.23	−0.70	GB6 J2203+1725	WNP
334.914	63.283	2.98	0.57	2.90	GB6 J2219+6317	NP
336.405	−5.002	3.43	0.26	−0.75	PMN J2225−0457	WNP
337.427	−8.582	2.69	0.30	−0.35	PMN J2229−0832	WNP
338.171	11.674	4.19	0.34	0.20	GB6 J2232+1143	WNP
338.909	−48.584	1.33	0.19	−0.85	PMN J2235−4835	WNP
341.600	−12.087	1.24	0.21	−1.05	PMN J2246−1206	WP
343.547	16.149	7.96	0.35	−0.35	GB6 J2253+1608	WNP
344.514	−28.003	3.58	0.28	−0.35	PMN J2258−2758	WNP
352.347	−47.438	1.18	0.22	−0.55	PMN J2329−4730	WP
359.607	−53.218	1.24	0.20	−0.60	PMN J2357−5311	WP

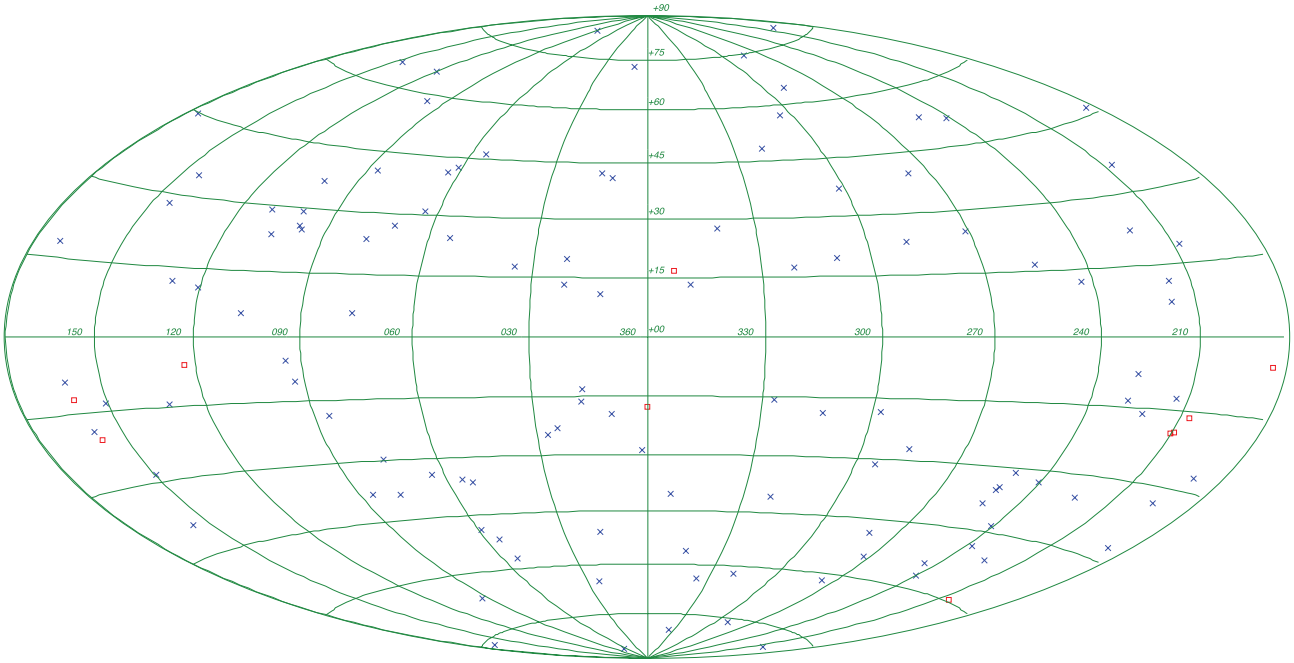

Figure 1. Position on the sky, in Galactic coordinates, of the 129 sources detected by the MMF at 61- and 94-GHz *WMAP* 7-year maps. Blue crosses represent the position of the 119 sources with confirmed counterparts in other catalogues (see Table 2); red squares represent the positions of the 10 Galactic or unidentified detections (see Table 1). A coloured version of this figure is available with the online edition of the paper.

4.5 Comparison with the *Planck* Early Release Compact Source Catalogue

Thanks to its higher sensitivity, *Planck* has detected far more sources than *WMAP*. The Early Release Compact Source Catalogue (ERCSC) lists 1381 sources detected at 100 GHz and 599 detected at 70 GHz; 308 and 788 of the ERCSC 70- and 100-GHz sources, respectively, are outside the *WMAP* Point Source Catalogue mask. Three of our sources in Table 2 are not present in the ERCSC, but are present in lower frequency catalogues with flux densities consistent with those inferred from *WMAP* data.

The ERCSC gives four different measures of flux density for each source. For the comparison with our results, we have chosen the estimate called FLUXDET, which is calculated using an approach similar to ours and appears to have higher reliability for low S/N values. Fig. 5 compares the FLUXDET flux densities at 70 and 100 GHz with the MMF ones at the nearest *WMAP* frequencies (61 and 94 GHz, respectively). Again, there is evidence that the MMF flux densities are affected by the Eddington bias below $\simeq$2 Jy. The MMF flux densities of the five sources with $S_{\mathrm{MMF,\,94\,GHz}} \gtrsim 8$ Jy are all lower than the ERCSC flux densities at 100 GHz. Two of these sources (the one at RA = 91.°968, Dec. = −6.°396 and Cen A) have a strong dust emission, seen in the *IRAS* survey, which enhances the 100-GHz flux density. The other three are well-known highly variable blazars (3C 273, 3C 279 and 3C 454.3), caught by *Planck* in a bright phase.

The spectral index distributions of our sources are pretty close to that of the ERCSC sources: the median spectral index of our sources is −0.65, with a standard deviation of 0.71; for ERCSC sources with $\gamma \leq 2$ (to avoid strong contamination by dust emission) and excluding the Galactic plane and the LMC region as defined

Downloaded from http://mnras.oxfordjournals.org/ at CSIC on January 9, 2015

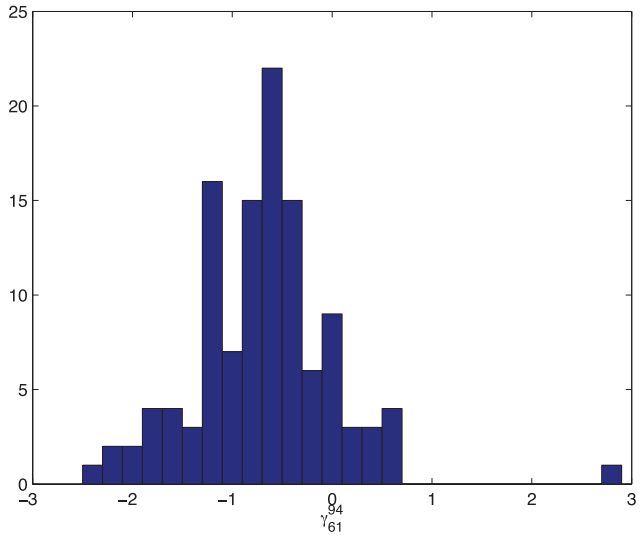

Figure 2. Spectral index distribution of sources in Table 2.

Table 3. Euclidean-normalized differential number counts at 61 and 94 GHz, based on our detections, in bins of $\Delta\log(S) = 0.2$ and taking into account the Bayesian correction to the flux densities.

S (Jy)	$S^{5/2}dN/dS$ (Jy$^{3/2}$ sr^{-1})	
	61 GHz	94 GHz
1.27	10.1 ± 1.7	10.9 ± 1.8
2.01	25 ± 4	18 ± 3
3.18	21 ± 5	19 ± 5
5.05	27 ± 8	9 ± 5
8.00	14 ± 8	18 ± 9
12.68	27 ± 16	9 ± 9
20.10	18 ± 18	18 ± 18
31.85	36 ± 36	–

previously in order to have a sample comparable with ours, we find a median value of −0.39 with a standard deviation of 0.52.

5 CONCLUSIONS

The detection of extragalactic point sources is a crucial task in the analysis of CMB maps because point sources are the main contaminant of the CMB power spectrum on small angular scales. From the same maps we can extract interesting astrophysical information about the point sources themselves. The development of efficient detection tools is therefore very important. The MMF holds the promise of achieving detections down to fainter flux densities than achievable by standard methods.

Applying this tool to 7-year *WMAP* maps at 61 and 94 GHz simultaneously, we have obtained 129 5σ detections at both frequencies, outside the Galactic plane (i.e. at $|b| > 5°$) and the LMC regions. Nine of these sources, listed in Table 1, either are known Galactic sources or reside in regions of high Galactic emission. One additional source, also listed in Table 1, does not have a counterpart in low-frequency radio catalogues. All the other 119 sources, listed in Table 2, do have a low-frequency counterpart; 104 of them reside outside the *WMAP* Point Source Catalogue mask. For comparison, the NEWPS 3-year catalogue contains 22 5σ detections at

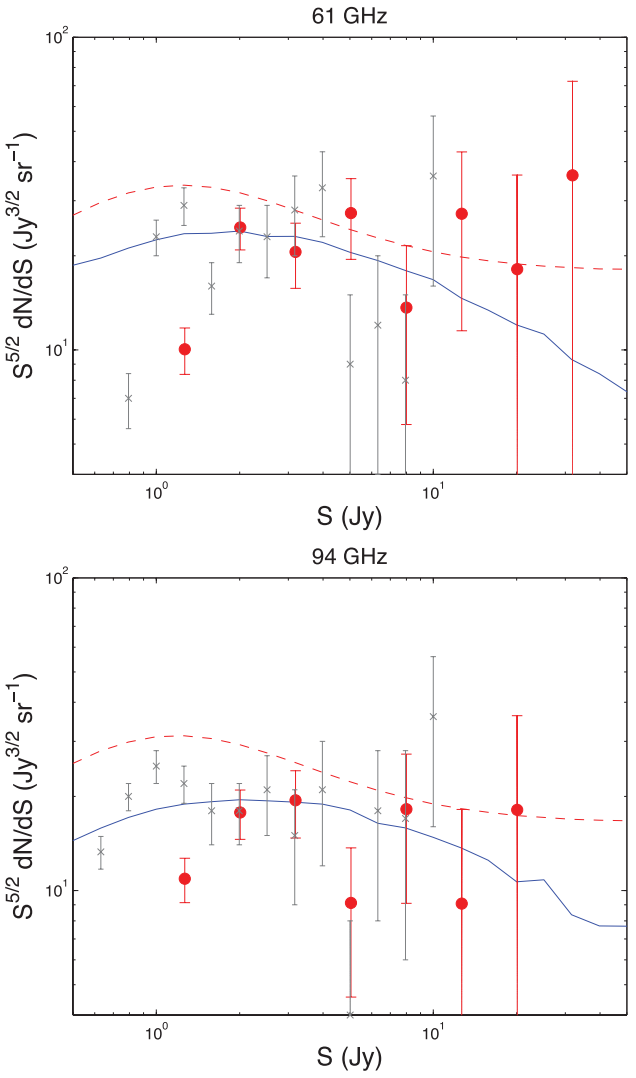

Figure 3. 7-year *WMAP* Euclidean-normalized differential number counts at 61 and 94 GHz based on the MMF sample (red points) with Poissonian error bars and the Bayesian correction to the flux densities. The grey crosses are the *Planck* counts at 70 and 100 GHz (Planck Collaboration 2011b). The solid lines are the prediction by the Tucci et al. (2011) model at 61 and 94 GHz, and the dashed lines are the prediction by the De Zotti et al. (2005) model at the same frequencies.

94 GHz. Although the *Planck* ERCSC contains far more sources at the frequencies (70 and 100 GHz) nearest to those used in the present analysis, we have detected three sources not present in the ERCSC, yet with flux densities consistent with lower frequency measurements.

A comparison of the flux densities yielded by the MMF with those obtained at ≃90 GHz with the ATCA or the NRAO 12-m telescope, and with the *Planck* ERCSC data at 70 and 100 GHz, shows a generally good agreement above ≃2 Jy, although the *rms* differences between MMF and ground-based or ERCSC values are larger than expected from variability and nominal measurement errors. This suggests that the errors associated with MMF flux density estimates are somewhat larger than the nominal values listed in Table 2. Below 2 Jy, the MMF flux densities tend to be somewhat overestimated, as the effect of the Eddington bias.

Downloaded from http://mnras.oxfordjournals.org/ at CSIC on January 9, 2015

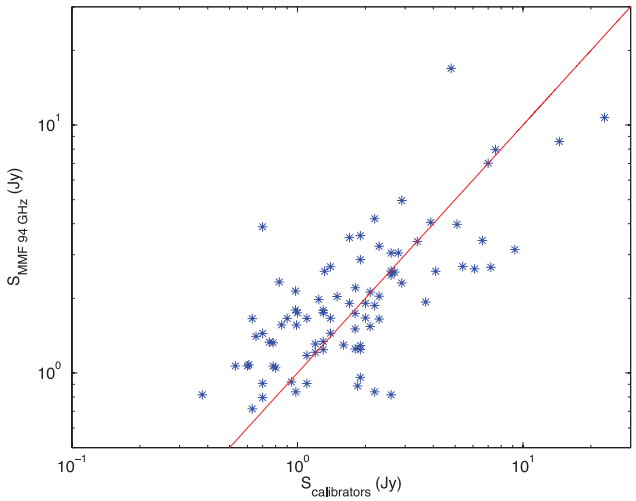

Figure 4. Comparison between 94-GHz flux densities recovered by the MMF and the ATCA (3-mm) and NRAO (90-GHz) flux density measurements, for the 85 sources in common. No correction for the slightly different frequencies of the sets of measurements was made. The solid line is $x = y$.

The distribution of 61–94 GHz spectral indices of sources in Table 2 has a median value equal to $\gamma_{61}^{94} = -0.65$ (with a dispersion of 0.71), while Wright et al. (2009), mostly based on lower frequency *WMAP* data, found a mean spectral index $\langle\gamma\rangle = -0.09$, with a dispersion $\sigma = 0.28$. Our results therefore confirm the steepening of extragalactic radio source spectra above ∼70 GHz, suggested by various data sets (González-Nuevo et al. 2008; Sadler et al. 2008; Massardi et al. 2010; Marriage et al. 2011) and then confirmed by analyses of different samples (Giommi et al. 2011; Planck Collaboration 2011b,c) of bright extragalactic sources extracted by the *Planck* ERCSC (Planck Collaboration 2011a).

This average steepening observed in the spectra of bright extragalactic sources, which are mainly blazars in this frequency range (Angel & Stockman 1980), has been recently interpreted by Tucci et al. (2011) in terms of the 'break' frequency, foreseen in the emission spectra of blazars by classic physical models for the synchrotron emission in the inner part of inhomogeneous conical jets. Remarkably, this new model by Tucci et al. (2011) is able to give a good fit not only to the source number counts presented here (see Fig. 3; Section 4.1), but also to almost all the published data on number counts and spectral index distributions of bright extragalactic radio sources up to, at least, 200–300 GHz.

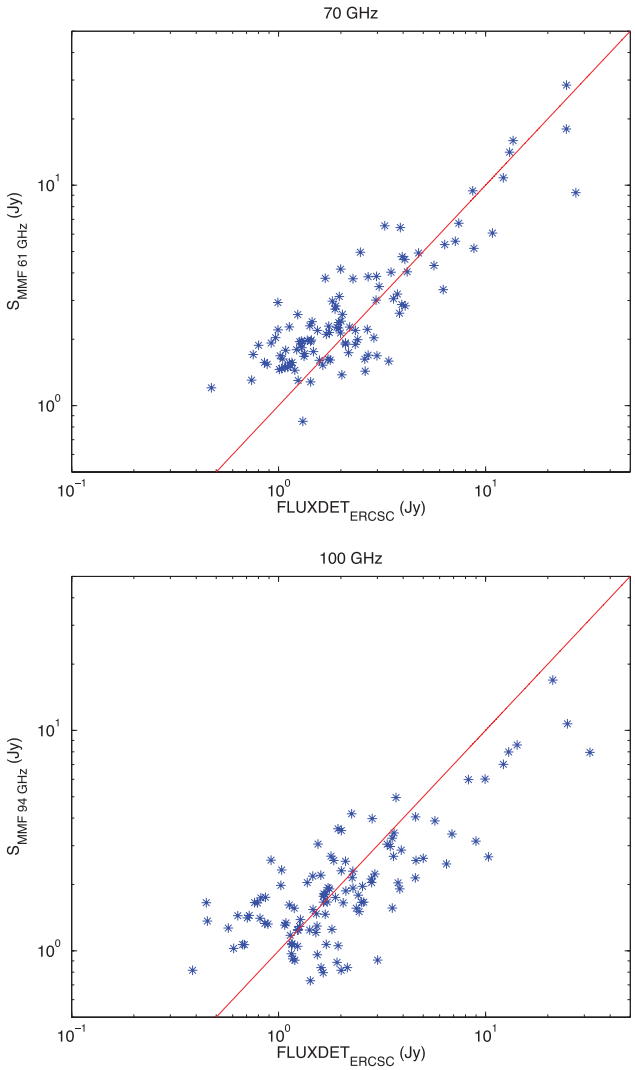

Figure 5. Comparison of the flux densities recovered by the MMF on *WMAP* maps at 61 and 94 GHz with the FLUXDET values reported in the *Planck* ERCSC at 70 GHz (upper panel) and 100 GHz (lower panel), respectively. The solid line is $x = y$.

ACKNOWLEDGMENTS

The authors acknowledge partial financial support from the Spanish Ministerio de Economía y Competitividad projects AYA2010-21766-C03-01 and CSD2010-00064. LFL acknowledges the Spanish CSIC for a JAE-Predoc fellowship and the hospitality of the Scuola Internazionale Superiore di Studi Avanzati (SISSA) of Trieste during two research stays in 2010 and 2011. ML-C thanks the Spanish Ministerio de Economía y Competitividad for a Juan de la Cierva fellowship. JG-N, GdZ, and MM acknowledge financial support from ASI/INAF Agreement I/072/09/0 for the *Planck* LFI activity of Phase E2. DH wishes to acknowledge the Spanish Ministerio de Educación for a José Castillejo Fellowship (JC2010-0096) and the Astronomy Group at the Cavendish Laboratory for their hospitality during a research stay in 2011. The authors are grateful to Luigi Toffolatti and Marco Tucci for their useful comments and explanations, in particular on the extragalactic source counts.

REFERENCES

Angel J. R. P., Stockman H. S., 1980, ARA&A, 18, 321
Argüeso F., Sanz J. L., Herranz D., 2011a, Signal Processing, preprint (arXiv:1101.0701v1)
Argüeso F., Salerno E., Herranz D., Sanz J. L., Kuruoğlu E. E., Kayabol K., 2011b, MNRAS, 414, 410
Barreiro R. B., Sanz J. L., Herranz D., Martínez-González E., 2003, MNRAS, 342, 119
Bennett C. L. et al., 2003, ApJ, 583, 1
Bertin E., Arnouts S., 1996, A&AS, 117, 393
Carvalho P., Rocha G., Hobson M. P., 2009, MNRAS, 393, 681
Chen X., Wright E. L., 2008, ApJ, 681, 747
Chiang L.-Y., Jørgensen H. E., Naselsky I. P., Naselsky P. D., Novikov I. D., Christensen P. R., 2002, MNRAS, 335, 1054
De Zotti G., Toffolatti L., Argüeso F., Davies R. D., Mazzotta P., Partridge R. B., Smoot G. F., Vittorio N., 1999, in Maiani L., Melchiorri F.,

Downloaded from http://mnras.oxfordjournals.org/ at CSIC on January 9, 2015

Vittorio N., eds, Proc. AIP Conf. Ser. Vol. 476, 3K Cosmology. Am. Inst. Phys., New York, p. 204
De Zotti G., Ricci R., Mesa D., Silva L., Mazzotta P., Toffolatti L., González-Nuevo J., 2005, A&A, 431, 893
Eddington A. S., 1913, MNRAS, 73, 359
Giommi P. et al., 2012, A&A, 541, A160
Gold B. et al., 2011, ApJS, 192, 15
González-Nuevo J., Argüeso F., López-Caniego M., Toffolatti L., Sanz J. L., Vielva P., Herranz D., 2006, MNRAS, 369, 1603
González-Nuevo J., Massardi M., Argüeso F., Herranz D., Toffolatti L., Sanz J. L., López-Caniego M., De Zotti G., 2008, MNRAS, 384, 711
Górski K. M., Hivon E., Banday A. J., Wandelt B. D., Hansen F. K., Reinecke M., Bartelmann M., 2005, ApJ, 622, 759
Herranz D., Sanz J. L., 2008, IEEE J. Selected Topics Signal Processing, 5, 727
Herranz D., Vielva P., 2010, IEEE Signal Processing Magazine, 27, 67
Herranz D., Gallegos J., Sanz J. L., Martínez-González E., 2002a, MNRAS, 334, 533
Herranz D., Sanz J. L., Hobson M. P., Barreiro R. B., Diego J. M., Martínez-González E., Lasenby A. N., 2002b, MNRAS, 336, 1057
Herranz D., Sanz J. L., López-Caniego M., González-Nuevo J., 2006, IEEE Int. Symp. Signal Processing Inf. Tech., 1, 541
Herranz D., López-Caniego M., Sanz J. L., González-Nuevo J., 2009, MNRAS, 394, 510
Hinshaw G. et al., 2007, ApJS, 170, 288
Hobson M. P., McLachlan C., 2003, MNRAS, 338, 765
Hobson M. P., Barreiro R. B., Toffolatti L., Lasenby A. N., Sanz J. L., Jones A. W., Bouchet F. R., 1999, MNRAS, 306, 232
Holdaway M., Owen F., Rupen M., 1994, Alma Memo #123, Source Counts at 90 GHz. National Radio Astronomy Observatory. Socorro, New Mexico, USA
Lanz L. F., Herranz D., Sanz J. L., González-Nuevo J., López-Caniego M., 2010, MNRAS, 403, 2120
López-Caniego M., Herranz D., Barreiro R. B., Sanz J. L., 2004, in Bouman C. A., Miller E. L., eds, Proc. SPIE Vol. 5299, Computational Imaging II. SPIE, Bellingham, p. 145
López-Caniego M., Herranz D., Sanz J. L., Barreiro R. B., 2005a, EURASIP J. Appl. Signal Processing, 15, 2426
López-Caniego M., Herranz D., Barreiro R. B., Sanz J. L., 2005b, MNRAS, 359, 993
López-Caniego M., Herranz D., González-Nuevo J., Sanz J. L., Barreiro R. B., Vielva P., Argüeso F., Toffolatti L., 2006, MNRAS, 370, 2047
López-Caniego M., González-Nuevo J., Herranz D., Massardi M., Sanz J. L., De Zotti G., Toffolatti L., Argüeso F., 2007, ApJS, 170, 108
López-Caniego M., Massardi M., González-Nuevo J., Lanz L., Herranz D., De Zotti G., Sanz J. L., Argüeso F., 2009, ApJ, 705, 868
Marriage T. A. et al., 2011, ApJ, 731, 100
Massardi M., López-Caniego M., González-Nuevo J., Herranz D., De Zotti G., Sanz J. L., 2009, MNRAS, 392, 733
Massardi M., Bonaldi A., Negrello M., Ricciardi S., Raccanelli A., De Zotti G., 2010, MNRAS, 404, 532
Planck Collaboration, 2011a, A&A, 536, A7
Planck Collaboration, 2011b, A&A, 536, A13
Planck Collaboration, 2011c, A&A, 536, A15
Sadler E. M., Ricci R., Ekers R. D., Sault R. J., Jackson C. A., de Zotti G., 2008, MNRAS, 385, 1656
Sanz J. L., Herranz D., Martínez-Gónzalez E., 2001, ApJ, 552, 484
Sanz J. L., Herranz D., López-Caniego M., Argüeso F., 2006, in Gini F., Kuruoglu E., eds, 14th Proc. EUSIPCO, Wavelets on the Sphere. Application to the Detection Problem. Hindawi Publishing Corporation, Pisa, p. 1
Sunyaev R. A., Zeldovich Y. B., 1970, Comments Astrophys. Space Phys., 2, 66
Sunyaev R. A., Zeldovich Y. B., 1972, Comments Astrophys. Space Phys., 4, 173
Tegmark M., de Oliveira-Costa A., 1998, ApJ, 500, L83
Toffolatti L., Argüeso Gómez F., De Zotti G., Mazzei P., Franceschini A., Danese L., Burigana C., 1998, MNRAS, 297, 117
Tucci M., Martínez-González E., Toffolatti L., González-Nuevo J., De Zotti G., 2004, MNRAS, 349, 1267
Tucci M., Martínez-González E., Vielva P., Delabrouille J., 2005, MNRAS, 360, 935
Tucci M., Toffolatti L., De Zotti G., Martínez-González E., 2011, A&A, 533, A57
Vielva P., Barreiro R. B., Hobson M. P., Martínez-González E., Lasenby A. N., Sanz J. L., Toffolatti L., 2001, MNRAS, 328, 1
Vielva P., Martínez-González E., Gallegos J. E., Toffolatti L., Sanz J. L., 2003, MNRAS, 344, 89
Vikhlinin A., Forman W., Jones C., Murray S., 1995, ApJ, 451, 542
Wright E. L. et al., 2009, ApJS, 180, 283

This paper has been typeset from a TEX/LATEX file prepared by the author.

Downloaded from http://mnras.oxfordjournals.org/ at CSIC on January 9, 2015